NASA Technical Paper 2930

1989

Auger Electron Intensity Variations in Oxygen-Charged Large Grain Polycrystalline Silver

W. S. Lee
Hampton University
Hampton, Virginia

R. A. Outlaw
Langley Research Center
Hampton, Virginia

G. B. Hoflund
and M. R. Davidson
University of Florida
Gainesville, Florida

National Aeronautics and Space Administration
Office of Management
Scientific and Technical Information Division

Summary

Auger electron spectroscopic studies of the grains in oxygen-charged polycrystalline silver show significant intensity variations as a function of crystallographic orientation. These intensity variations have been observed in studies of the Auger images and line scans of the different grains (randomly selected) for each silver transition energy. The results can be attributed to the diffraction of the ejected Auger electrons and interpreted by corresponding changes in the electron mean free path for inelastic scattering and by oxygen atom accumulation in the subsurface. The subsurface (second layer) octahedral sites have increased in size because of surface relaxation and serve as a stable reservoir for the dissolved oxygen.

Introduction

Auger electron spectroscopy (AES) has found wide acceptance as a quantitative or semiquantitative method for elemental analysis of solid surfaces (refs. 1–12), but most papers on quantitative measurements have totally ignored the possibility of diffraction of both Auger electrons escaping from the surface and incident electrons used for the initial excitation. Because the cylindrical mirror analyzer (CMA) has a relatively large collection angle, diffraction and other possible effects associated with an inherent angular dependence of Auger electron emission might be expected to average out.

According to the simplified theory of Auger yield proposed by Bishop and Riviere (ref. 3), Auger signals from a clean substrate should be independent of the crystallographic orientation for several reasons: (1) the change in the density of the atomic planes parallel to the surface is partially offset by a compensating change in layer spacing, (2) the angular dependence of Auger electron emission from single-crystal surfaces and from adsorbates on single-crystal surfaces, and (3) the direction of the incident electron beam and the direction along which Auger electrons are collected. These questions have been the subject of several experimental and theoretical investigations (refs. 13–35). The general conclusions from these works appear to be that a strong crystallographically associated angular dependence of Auger electron emission arises from the combination of inherent anisotropic electron emission of the bulk atoms, diffraction effects in the single crystal, and channeling effects leading to variations in the incident electron flux (sometimes referred to as Kikuchi correlation or inverse Kikuchi effects). Actually, there is no direct method available to distinguish between these contributions.

In this paper, the relative intensity of the silver and oxygen Auger peaks from different grains of an oxygen-charged polycrystalline silver sample was investigated by Auger images and line scans with the intent of examining the Auger intensity variation as a function of crystallographic orientation.

Experimental

The experimental system is comprised of a standard ultrahigh vacuum (UHV) work chamber pumped by a 150 L/s ion pump and a titanium sublimation pump (base pressure is around 2×10^{-12} torr). The system is equipped with a four-grid optics system for low energy electron diffraction (LEED), a 10-kV cylindrical mirror analyzer for AES with an electron beam size of approximately 2 μm, a quadrupole mass spectrometer for residual gas analysis, and several ion and electron guns. A schematic top view of the system is shown in figure 1.

The sample (0.999999+ vacuum-melted Ag) used in this work was spark machined from large grain silver (grain diameters are in the range of 1–5 mm) in the shape of a 5 mm square, 0.254 mm thick. The sample was prepared by ultrasonic cleaning in detergent, rinsing in deionized water, and hot air drying, and then it was installed into the sample introduction/preparation chamber, shown in figure 1.

The silver sample was mounted on the sample holder and then installed into the threaded carousel through the sight port. The sample was screwed into the slot, where the sample back initially contacts the spring-loaded thermocouple, which is depressed until the sample back contacts the heater electrode. The heater assembly, shown in figure 2, is designed to heat the sample to greater than 1000°C in a selected environment (ultrahigh vacuum to a pressure of several atmospheres). The sight port was closed, and the system was initially evacuated by a molecular drag pump and then subsequently pumped by a 60 L/s ion pump. The pressure in the sample transfer volume was monitored by either the capacitance manometer or an ion gauge. A 150°C overnight bakeout of the sample transfer volume produced a pressure in the 10^{-9}-torr range. The sample was then heated to 600°C for 2 hr, cooled to room temperature, and then backfilled with oxygen to 100 torr and reheated to 600°C for 2 hr. The sample temperature of 600°C was to maximize the solubility of oxygen in silver because the desorption of oxygen from the silver membrane (vacuum on both sides) occurs at 630°C (ref. 36). After charging the silver with oxygen, the sample was then transferred from the carousel to the transfer rod by engaging the two pins on the rod into the holes on the sample

holder and rotating the external magnet to disengage. The carousel was then retracted to clear the transfer path. The isolation valve was then opened to vacuum connect the preparation chamber to the UHV analysis chamber. The transfer rod with sample holder and sample was then extended into the UHV chamber, where the sample was installed into the threaded manipulator-receiving block. The manipulator used in our system has a right angle 2.5 in. offset and flip mechanism with similar heating capability to that in the introduction/preparation chamber. The transfer rod was then disengaged, retracted into the sample transfer chamber, and the isolation valve closed. The sample could then be quickly positioned in front of the desired diagnostic instrument to begin the analysis. The random grains selected for study were analyzed by Laue back diffraction techniques to determine their orientation. A metal mask was used to reduce the size of the Cu $K\alpha$ beam to less than 0.5 mm. The grain size was on average about 2 mm, so the beam was completely intercepted by each individual grain. The sample was positioned by a vernier stage to the selected grains of interest, where the diffraction pattern was captured on film. Figure 3 shows a tracing of the grain structure in the region studied, specifically the (421) and (221) grains. The (221) grain is only about 15° off the (111) pole. The grain boundary at the top of the tracing is probably a tilt or twist boundary. The (421) grain appears to be rotated about 90° from the $[\bar{1}10]$ direction of the (221).

Results and Discussion

An AES analysis of the oxygen-charged silver in 100 torr oxygen at 600°C for 2 hr showed some small concentration of carbon and oxygen. After a brief argon ion bombardment, a representative Auger spectrum of the clean oxygen-charged silver is as shown in figure 4. Note here that the 351-eV and the 355-eV peaks are not resolved. This is because a modulation of 10 V was used to sufficiently increase the sensitivity so that the oxygen peak at 503 eV could be detected. The oxygen-to-silver peak ($M_{4,5}VV$ 355 eV) ratio is around 4 percent, which is in good agreement with the results of Rovida et al. (refs. 37 and 38). They found a ratio of up to 4 percent on both Ag (111) and Ag (110) single-crystal surfaces.

Figure 5 shows Auger images and line scans of silver and oxygen after a brief cleaning by argon ion bombardment (figs. 5(a) and (b)) and after a subsequent anneal for 30 min (figs. 5(c) and (d)). Figure 5(a) shows that there is a significant silver contrast and intensity variation between grains of the sample, clearly showing the effects of crystalline orientation. The grain orientations are shown in figure 3. Figure 5(b), which represents the dissolved oxygen image and line scan, does not show any significant contrast. After heating the sample at 470°C at 1×10^{-11} torr for 30 min, the damage incurred by ion bombardment was annealed out, and the contrast shown in figure 5(c) was correspondingly greater. (Compare fig. 5(c) with fig. 5(a).) The anneal, however, did not significantly improve the dissolved oxygen contrast between the grains (fig. 5(d)) but did appear to concentrate more oxygen at the surface. These results indicate that the intensity of the silver Auger peak depends on (1) the crystallographic orientation and (2) the surface order of the grains. Further, the fact that the oxygen does not appear to have significantly changed in either case, presumably because it is randomly distributed throughout the interstitial sites of the silver, provides additional evidence for the crystalline order dependence.

Chang (ref. 21) has studied the diffraction effects of the O KLL, Si KLL, and Si LVV peaks from a Si (111) surface with approximately 10 Å oxide. He found that the decrease of the Si KLL (1620 eV) Auger peak is about a factor of 2 upon rotation from 0° (normal incidence of the primary electron beam) to 5°, but that the Si LVV (92 eV) peak is only slightly decreased. The O KLL and the Si LVV peaks did not change appreciably upon rotation because they originated in an amorphous oxide material. This work indicates the magnitude of the diffraction and contrast effects in a polycrystalline material. In silver, the heat of formation of bulk silver oxide ($\approx$14.5kcal/molO_2) (ref. 39) is smaller than the heat of adsorption for the oxygen atom on silver ($\approx$42.4 kcal/mol O_2) (ref. 39), so oxygen atoms are much more stable in a chemisorbed state than in bulk silver oxide. More specifically, the oxygen appears to reside in subsurface sites and, as observed by LEED experiments, in no particular order (ref. 40), so there may be no significant diffraction effects.

Becker and Hagstrum (ref. 41), McDonnell et al. (ref. 42), and Thapliyal and Unertl (ref. 43) found that most Auger electron diffraction peaks for well-ordered Ni (100), Cu (100), and Cu (111) surfaces have the following characteristics:

1. Appear only for transition energies between 100–400 eV.
2. Independent of the angle of incidence of the primary electron beam.
3. Unique function of temperature. (These peaks strongly decrease at elevated temperature, indicating a loss of order and therefore a reduction of diffraction.)

4. Significant decrease in height with increasing incident electron beam energy.
5. Strongly dependent on clean and well-ordered surfaces. (A small amount of disorder in the adsorbed layer induced by weak ion bombardment (reduced current and short time) almost completely destroyed these peaks, but the peaks remained undiminished as long as the overlayer is ordered.)

Therefore, O *KLL* Auger electrons may not diffract because the oxygen peak energy (503 eV) is large compared with the diffraction peak energies as indicated by (1) above.

Further, it is assumed that most of the oxygen atoms are located in the octahedral interstitial sites of the silver because the radii of octahedral sites (r_{oct} = 0.598 Å) are larger than those of the tetrahedral sites (r_{tet} = 0.325 Å) of the fcc structure and also are comparable to the radii of the oxygen atoms ($r_{oxy} \approx$ 0.6 Å). These interstitial regions are also affected by surface relaxation (refs. 44–50). Relaxation, such as expansions and contractions, does not change the two-dimensional lattice but does change in the z-direction. The varying layer spacing normal to the surface exhibits a damped oscillatory size distribution. It is likely that most oxygen atoms will be located between the second and third layers because the spacing between the first and second layers is generally contracted, and the spacing between the second and third is generally expanded. An accumulation of oxygen atoms between the second and third layers will not change the crystalline order because the radius of the octahedral site in this region is larger than that of the oxygen atom because of surface relaxation. If it is assumed that diffraction is significantly connected to the electron mean free path (EMFP) for inelastic scattering, then the O *KLL* Auger electrons emitted from these sites are probably not influenced by diffraction because oxygen Auger electrons (EMFP ≈10 Å) emitted between the second and third layers are so close to the surface ($d \approx$ 4 Å).

Figure 6 shows the variation of oxygen-to-silver ($M_{4,5}VV$) peak ratio for the grains presented in figure 5. The oxygen-to-silver ratio obtained after cleaning by ion bombardment is around 3.7 percent (fig. 6, solid circles). There is no change of ratio with different grains. The relatively small effect of sputtering for different grains of silver is not observed here because of scale. The oxygen-to-silver ratio obtained after heating at 470°C in UHV for 30 min, however, is different for the different grains (fig. 6, open circles), hereinafter referred to as (421) and (221) grains, respectively. The oxygen-to-silver ratio is around 10.8 percent in the (421) grain and 9.1 percent in the (221) grain. This difference comes from the intensity variation of the silver Auger peak with different grains, as shown in figure 5, because the oxygen Auger intensity did not change. The significant change of the oxygen-to-silver ratio between cleaning by ion bombardment and heating probably can be explained by the amount of oxygen located below the surface increasing with increasing temperature. This result also indicates that the intensity variation of the silver ($M_{4,5}VV$) peak is independent of the amount of oxygen near the surface.

Figure 7 shows images and line scans of different Auger transition energies of silver after heating the sample at 470°C in UHV for 30 min. The contrast of the Auger images of silver on different grains shows a strong dependence on the different transition energies of silver. The highest contrasts are shown in figures 7(a) and 7(e), the $M_{4,5}VV$ (355 eV) and $N_1N_{2,3}V$ (27 eV) transitions, respectively. The lowest contrast is shown in figure 7(c), the $M_{4,5}N_1V$ (265 eV) transition. Moderate contrasts are shown in figures 7(b) and 7(d), the $M_{4,5}N_{2,3}V$ (303 eV) or N_1VV (78 eV) transitions, respectively. Diffraction effects of Auger electrons with short EMFP might be expected to be minimal because only atoms close to the surface contribute to the observed Auger peak. As shown in table I, the EMFP of the Ag $N_{2,3}VV$ (47 eV), N_1VV (78 eV), and $M_{4,5}N_1V$ (265 eV) transitions are smaller than those of the Ag $N_1N_{2,3}V$ (27 eV), $M_{4,5}N_{2,3}V$ (303 eV), and $M_{4,5}VV$ (355 eV) transitions. Although the EMFP of Ag N_1VV is the smallest, the intensity variation over the different grains is greater than those of Ag $N_{2,3}VV$ and $M_{4,5}N_1V$. Figure 8 shows the low energy region (20 eV–100 eV) for the (421) grain and the (221) grain. The N_1VV intensity is significantly increased from the (421) grain to the (221) grain and is comparable with the $N_{2,3}VV$ (47 eV) intensity. This may be explained by the correlation of the Auger electron wavelength with the atomic radius (ref. 53). The wavelength of the Ag N_1VV (78 eV) electron is 1.39 Å. The Ag (110) surface corresponds to the largest multilayer relaxation because of the most open low-index surface. Kuk and Feldman (ref. 48) have measured the spacing between the first and third layers, which represents the nearest-neighbor spacing at the Ag (110) surface, and found it to be 2.79 Å compared with the bulk value of 2.89 Å. However, the chance of diffraction of the Ag N_1VV (78 eV) electrons may be very high because the wavelength of the Auger emission is, within experimental error, equal to half the spacing between the first and third layers. Second-order diffraction (2 × 1.39 Å) is in good accord with the nearest-neighbor spacing (2.79 Å) of the Ag (110) surface.

In figure 8, the X (65 eV) peak shows a large intensity variation with different grains that has not been identified, but it may be an artifact due to the diffraction effects.

Noonan et al. (ref. 16) and Matsudaira and Onchi (ref. 27) found that the angular distribution of Auger electron emission from clean Cu (100) and Ag (100) single-crystal surfaces is independent of Auger transition. They measured the angular intensity variation of the Cu $M_{2,3}VV$ (62 eV) and Cu M_1VV (107 eV) transitions from Cu (100), and the Ag $M_{4,5}VV$ (355 eV), Ag $M_{4,5}N_{2,3}V$ (303 eV), Ag $M_{4,5}N_1V$ (265 eV), and Ag $N_{2,3}VV$ (47 eV) Auger electrons from Ag (100) as a function of either θ or ϕ (where θ is the polar angle and ϕ is the azimuthal angle in the crystal surface). Matsudaira and Onchi (ref. 27) showed that angular distributions of Auger electron emission with different transitions have a similar trend, with some maxima located near the low-index crystallographic directions, and explained that these intense peaks (355-, 303-, and 265-eV Ag peaks) correspond with the low-index directions and suggested the contribution of diffraction effects with Kikuchi correlation instead of the initial inherent anisotropic effect. But they obtained a much different trend of the Ag $N_{2,3}VV$ (47 eV) Auger peak, and this discrepancy has been interpreted by the extended multiple scattering theory with consideration of initial state anisotropy in the Auger transition. As shown in figure 8, the Ag $N_{2,3}VV$ (47 eV) peak does not show a significant intensity change on different grains compared with Ag $N_1N_{2,3}V$ (27 eV) and Ag N_1VV (78 eV). These results probably can be explained, as previously discussed, by the EMFP for inelastic scattering and the correlation of the Auger electron wavelength with the layer spacing. So we may conclude that the variation of the Auger signal intensity from grain to grain in polycrystalline silver strongly depends on the transition energies because they have different EMFP's. Bishop et al. (ref. 32) observed large crystallographic effects in polycrystalline copper and silver and suggested that the anisotropic emission of the Auger electrons contributes less to this effect than the electron channeling which comes from changes in the surface ionization as a result of diffraction of the incident electron beam. The effects of anisotropic emission are often largely averaged over the input aperture of the electron analyzer, but the contribution from electron channeling is not averaged and can be quite large. Sakai and Mogami (ref. 33) studied the variation of the Auger signal from grain to grain in a polycrystalline aluminum sample, using channeling patterns appearing in a scanning Auger electron image observation. They obtained both the Al KLL Auger electron channeling pattern (ECP) and the backscattered ECP for the three different grains, where the contrasts result from the Al KLL Auger electron and the backscattered electrons, respectively. They emphasized that the main contribution to the variation of Auger intensity on the different grains is due to the backscattered electrons, because both the Auger ECP and the backscattered ECP obtained in the same grains yield exactly the same channeling contrast even though the contrast of Al KLL Auger ECP images is less than that of the backscattered electrons. Futhermore, they also observed that the intensity variation of the Al KLL (1396 eV) peak is larger than that of the Al LVV (68 eV). This result probably can be explained by the EMFP, because the Al KLL ($\approx$27 Å) Auger electrons have a much longer EMFP than that of Al LVV ($\approx$4 Å) (ref. 51).

Actually, there are no general rules for predicting which one will be the major contribution to variation of the Auger signal from the different crystallographic orientations because there is no direct method available to distinguish between these different contributions. Although both diffraction of the incident electron beam and backscattered electron flux affect the Auger electron generation, the largest crystallographic effects observed in this work were attributed to diffraction of the emitted Auger electrons.

Conclusions

Auger intensity variations over an oxygen-charged polycrystalline silver surface have been observed by studies of Auger images and line scans of randomly selected adjacent grains. It has been found that the intensity of silver Auger peaks is very strongly dependent upon the crystallographic orientation, the order of the grains, and the specific transition energy. The observations are primarily because of the diffraction of ejected Auger electrons. The Ag N_1VV (78 eV) peak has the smallest electron mean free path (EMFP) and strongly depends on crystallographic orientation and order because of the close correlation of the EMFP with the layer spacing of the silver (high probability of diffraction).

The O KLL peak, having a large EMFP compared with silver, is independent of crystallographic orientation of grains because most of the oxygen atoms are randomly located in the subsurface of silver. The increased size of the octahedral sites in the subsurface (second layer) occurs because of surface relaxation and serves as a stable reservoir for the dissolved oxygen.

NASA Langley Research Center
Hampton, VA 23665-5225
August 4, 1989

References

1. Lander, J. J.: Auger Peaks in the Energy Spectra of Secondary Electrons From Various Materials. *Phys. Review,* vol. 91, no. 6, Sept. 15, 1953, pp. 1382–1387.
2. Harris, L. A.: Analysis of Materials by Electron-Excited Auger Electrons. *J. Appl. Phys.,* vol. 39, no. 3, Feb. 15, 1968, pp. 1419–1427.
3. Bishop, H. E.; and Riviere, J. C.: Estimates of the Efficiencies of Production and Detection of Electron-Excited Auger Emission. *J. Appl. Phys.,* vol. 40, no. 4, Mar. 15, 1969, pp. 1740–1744.
4. Seah, M. P.: Quantitative Auger Electron Spectroscopy and Electron Ranges. *Surf. Sci.,* vol. 32, no. 3, Sept. 1972, pp. 703–728.
5. Palmberg, Paul W.: Quantitative Analysis of Solid Surfaces by Auger Electron Spectroscopy. *Anal. Chem.,* vol. 45, no. 6, May 1973, pp. 549A–550A, 552A, 554A, and 556A.
6. Chang, Chuan C.: Analytical Auger Electron Spectroscopy. *Characterization of Solid Surfaces,* Philip F. Kane and Graydon B. Larrabee, eds., Plenum Press, c.1974, pp. 509–575.
7. Palmberg, Paul W.: Quantitative Auger Electron Spectroscopy Using Elemental Sensitivity Factors. *J. Vac. Sci. & Technol.,* vol. 13, no. 1, Jan./Feb. 1976, pp. 214–218.
8. Holloway, Paul H.: Fundamentals and Applications of Auger Electron Spectroscopy. *Advances in Electronics and Electron Physics,* Volume 54, L. Marton and C. Marton, eds., Academic Press, Inc., 1980, pp. 241–298.
9. Powell, C. J.: The Physical Basis for Quantitative Surface Analysis by Auger Electron Spectroscopy and X-Ray Photoelectron Spectroscopy. *Quantitative Surface Analysis of Materials,* N. S. McIntyre, ed., ASTM Spec. Tech. Publ. 643, c.1978, pp. 5–29.
10. Prutton, M.: How Quantitative Is Analysis in the Scanning Auger Electron Microscope? *Scanning Electron Microsc.,* vol. 1982, pt. I, pp. 83–91.
11. Powell, C. J.; Erickson, N. E.; and Madey, T. E.: Results of a Joint Auger/ESCA Round Robin Sponsored by ASTM Committee E-42 on Surface Analysis—Part II, Auger Results. *J. Electron Spectrosc. & Relat. Phenom.,* vol. 25, no. 2–3, Feb. 1982, pp. 87–118.
12. Seah, M. P.; and Holbourn, M. W.: Quantitative AES: The Problems of the Energy Dependent Phase Shift and Modulation Amplitude and of the Non-Ideal Behaviour of the Channel Electron Multiplier. *J. Electron Spectrosc. & Relat. Phenom.,* vol. 42, no. 3, Apr. 1987, pp. 255–269.
13. McDonnell, L.; and Woodruff, D. P.: Angular Dependence of Auger Electron Emission From a Single Crystal Specimen. *Vacuum,* vol. 22, no. 10, Oct. 1972, pp. 477–480.
14. Holland, B. W.; McDonnell, L.; and Woodruff, D. P.: Angular Dependence of Auger Electron Emission From Solid Surfaces. *Solid State Commun.,* vol. 11, no. 8, Oct. 15, 1972, pp. 991–993.
15. McDonnell, L.; Woodruff, D. P.; and Holland, B. W.: Angular Dependence of Auger Electron Emission From Cu (111) and (100) Surfaces. *Surf. Sci.,* vol. 51, no. 1, July 1975, pp. 249–269.
16. Noonan, J. R.; Zehner, D. M.; and Jenkins, L. H.: Angular-Resolved Auger Emission Spectra From a Clean Cu (100) Surface. *J. Vac. Sci. Technol.,* vol. 13, no. 1, Jan./Feb. 1976, pp. 183–187.
17. Zehner, D. M.; Noonan, J. R.; and Jenkins, L. H.: Angular Effects in Auger Electron Emission From Cu (110). *Solid State Commun.,* vol. 18, no. 4, 1976, pp. 483–486.
18. Matsudaira, T.; Watanabe, M.; and Onchi, M.: Angular Distribution of Auger Electron Emission From Clean and Gas-Covered Fe (100) Surfaces. *Japanese J. Appl. Phys.,* suppl. 2, pt. 2, 1974, pp. 181–184.
19. Weeks, S. P.; and Liebsch, A.: Comparison of Angular Resolved Measurements of Auger Emission From a Clean Nickel (100) Surface With Electron Multiple Scattering Calculations. *Surf. Sci.,* vol. 62, no. 1, Jan. 1977, pp. 197–205.
20. Allie, G.; Blanc, E.; and Dufayard, D.: Angular Distribution of the Auger Emission From Aluminum and Nickel Surfaces. *Surf. Sci.,* vol. 57, no. 1, July 1, 1976, pp. 293–305.
21. Chang, C. C.: Intensity Variations in Auger Spectra Caused by Diffraction. *Appl. Phys. Lett.,* vol. 31, no. 4, Aug. 15, 1977, pp. 304–306.
22. White, S. J.; Woodruff, D. P.; and McDonnell, L.: Angular Dependence of Auger Electron Emission From Si and Cu(100) Surfaces in the Presence of Overlayers. *Surf. Sci.,* vol. 72, no. 1, Mar. 1, 1978, pp. 77–83.
23. Rusch, T. W.; Bertino, J. P.; and Ellis, W. P.: Kikuchi Correlations in Auger Electron Spectroscopy. *Appl. Phys. Lett.,* vol. 23, no. 7, Oct. 1, 1973, pp. 359–360.
24. Rusch, T. W.; and Ellis, W. P.: High-Angular-Resolution Secondary-Electron Spectroscopy: Kikuchi Correlations for As(0001). *Appl. Phys. Lett.,* vol. 26, no. 2, Jan. 15, 1975, pp. 44–46.
25. Baines, M.; Howie, A.; and Andersen, S. Kjaer: Crystalline Effects in Backscattering and Auger Production. *Surf. Sci.,* vol. 53, Dec. 1975, pp. 546–553.
26. Armitage, A. F.; Woodruff, D. P.; and Johnson, P. D.: Crystallographic Incident Beam Effects in Quantitative Auger Electron Spectroscopy. *Surf. Sci.,* vol. 100, no. 2, 1980, pp. L483–L490.
27. Matsudaira, T.; and Onchi, M.: Angle-Resolved Auger Emission From Ag(100) Surface. *Surf. Sci.,* vol. 74, no. 3, June 11, 1978, pp. 684–688.
28. Mosser, A.; Burggraf, C. N.; Goldsztaub, S.; and Ohtsuki, Y. H.: LEED Kikuchi Pattern: Phonon and Plasmon Contributions. *Surf. Sci.,* vol. 54, no. 3, Mar. 1976, pp. 580–592.
29. Place, J. D.; and Prutton, M.: Angular Dependence of Auger Electron Emission From MgO and NiO. *Surf. Sci.,* vol. 82, no. 2, Apr. 1, 1979, pp. 315–332.
30. Ichinokawa, T.; LeGressus, C.; Mogami, A.; Pellerin, F.; and Massignon, D.: Variation of Relative Intensities Between Surface and Bulk Plasmon Losses Due to Crystal Orientations for Aluminum in Low Energy Electron Reflection Loss Spectroscopy. *Surf. Sci.,* vol. 111, no. 1, Oct. 11, 1981, pp. L675–L679.
31. Doern, F. E.; Kover, L.; and McIntyre, N. S.: Channelling Effects in Polycrystalline Copper. A Serious Impediment

to Quantitative Auger Analysis? *Surf. & Interface Anal.*, vol. 6, no. 6, Dec. 1984, pp. 282–285.

32. Bishop, H. E.; Chornik, B.; LeGressus, C.; and LeMoel, A.: Crystalline Effects in Auger Electron Spectroscopy. *Surf. & Interface Anal.*, vol. 6, no. 3, June 1984, pp. 116–128.
33. Sakai, Y.; and Mogami, A.: Summary Abstract: Influence of Crystalline Grain Orientation of Auger Electron Spectroscopy. *J. Vac. Sci. & Technol.*, vol. A4, no. 3, May/June 1986, pp. 1563–1565.
34. Bennett, B.; and Viefhaus, H.: Electron Channelling Induced Effects in Grain Boundary AES Measurements. *Surf. & Interface Anal.*, vol. 8, no. 3, June 1986, pp. 127–132.
35. Sakai, Y.; and Mogami, A.: Summary Abstract: Observation of Auger Electron Channeling Pattern and Eliminating Method of Crystal Orientation Dependency in Quantitative Auger Electron Spectroscopy. *J. Vac. Sci. & Technol.*, vol. A5, no. 4, July/Aug. 1987, pp. 1222–1224.
36. Outlaw, R. A.; Sankaran, S. N.; Hoflund, G. B.; and Davidson, M. R.: Oxygen Transport Through High-Purity, Large-Grain Ag. *J. Mater. Res.*, vol. 3, no. 6, Nov.–Dec. 1988, pp. 1378–1384.
37. Rovida, G.; and Pratesi, F.; Maglietta, M.; and Ferroni, E.: Chemisorption of Oxygen on the Ag(111) Surface. *Surf. Sci.*, vol. 43, no. 1, May 1974, pp. 230–256.
38. Rovida, G.; and Pratesi, F.: Chemisorption of Oxygen on the Silver (110) Surface. *Surf. Sci.*, vol. 52, no. 3, Nov. 1975, pp. 542–555.
39. Campbell, Charles T.: Atomic and Molecular Oxygen Adsorption on Ag(111). *Surf. Sci.*, vol. 157, no. 1, July 1985, pp. 43–60.
40. Zanazzi, E.; Maglietta, M.; Bardi, U.; Jona, F.; and Marcus, P. M.: Test of Structural Models for Ag(110) $1 \times 2-0$ by LEED Intensity Analysis. *J. Vac. Sci. & Technol.*, vol. 1, no. 1, Jan.–Mar. 1983, pp. 7–11.
41. Becker, G. E.; and Hagstrum, H. D.: Diffraction Peaks in Secondary-Electron Energy Spectra. *J. Vac. Sci. & Technol.*, vol. 11, no. 1, Jan./Feb. 1974, pp. 284–287.
42. McDonnell, L.; Powell, B. D.; and Woodruff, D. P.: Temperature Dependent Peaks in Secondary Electron Emission Spectra. *Surf. Sci.*, vol. 40, no. 3, Dec. 1, 1973, pp. 669–682.
43. Thapliyal, H. V.; and Unertl, W. N.: Diffraction Features in Secondary Electron Emission. *J. Vac. Sci. & Technol.*, vol. 16, no. 2, Mar./Apr. 1979, pp. 523–526.
44. Smith, John R.; and Banerjea, Anitava: Summary Abstract: Theory of the Oscillatory Relaxation of Face-Centered-Cubic (110) Surfaces. *J. Vac. Sci. & Technol.*, vol. A6, no. 3, May/June 1988, pp. 812–814.
45. Yalisove, S. M.; and Graham, W. R.: Medium-Energy Ion Scattering Studies of Relaxation at Metal Surfaces. *J. Vac. Sci. & Technol.*, vol. A6, no. 3, May/June 1988, pp. 588–596.
46. Foiles, S. M.; Baskes, M. I.; and Daw, M. S.: Embedded-Atom-Method Functions for fcc Metals Cu, Ag, Au, Ni, Pd, Pt and Their Alloys. *Phys. Review*, vol. B33, no. 12, June 15, 1986, pp. 7983–7991.
47. Jiang, P.; Marcus, P. M.; and Jona, F.: Relaxation at Clean Metal Surfaces. *Solid State Commun.*, vol. 59, no. 5, Aug. 1986, pp. 275–280.
48. Kuk, Y.; and Feldman, L. C.: Oscillatory Relaxation of the Ag(110) Surface. *Phys. Review*, vol. B30, no. 10, Nov. 15, 1984, pp. 5811–5816.
49. Sokolov, J.; Jona, F.; and Marcus, P. M.: Trends in Metal Surface Relaxation. *Solid State Commun.*, vol. 49, no. 4, Jan. 1984, pp. 307–312.
50. Finnis, M. W.; and Heine, V.: Theory of Lattice Contraction at Aluminum Surfaces. *J. Phys. F*, vol. 4, no. 3, Mar. 1974, pp. L37–L41.
51. Penn, David R.: Electron Mean-Free-Path Calculations Using a Model Dielectric Function. *Phys. Review*, vol. B35, no. 2, Jan. 15, 1987-I, pp. 482–486.
52. Palmberg, P. W.; and Rhodin, T. N.: Auger Electron Spectroscopy of fcc Metal Surfaces. *J. Appl. Phys.*, vol. 39, no. 5, Apr. 1968, pp. 2425–2432.
53. Barthes, M. G.; and Rhead, G. E.: Substrate and Instrumental Effects in Quantitative Auger Electron Spectroscopy: The System Lead on Gold. *J. Phys. D: Appl. Phys.*, vol. 13, no. 5, May 14, 1980, pp. 747–757.

Table I. Electron Mean Free Path for Inelastic Scattering

Auger transition energies of silver	$N_1N_{2,3}V$ (27 eV)	$N_{2,3}VV$ (47 eV)	N_1VV (78 eV)	$M_{4,5}N_1V$ (265 eV)	$M_{4,5}N_{2,3}V$ (303 eV)	$M_{4,5}VV$ (355 eV)	Reference number
Electron mean free			4		7	8	52
path for inelastic	10	5.4	4.3			8.5	(a)
scattering, Å	8	6	5	6		7.5	51

[a]This information was given by J. C. Tracy, NATO Summer School Lectures, Gent, Belgium, 1972.

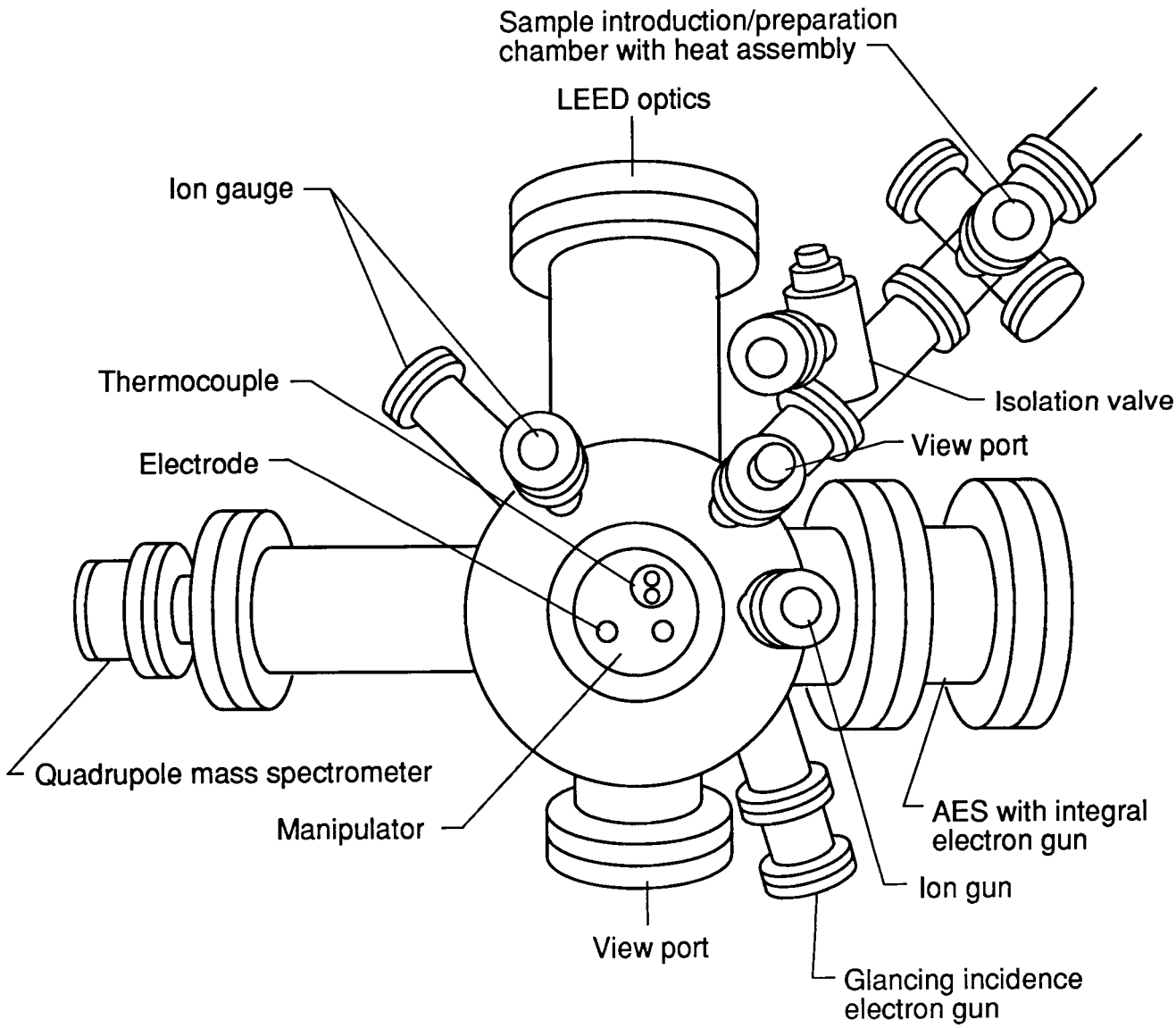

Figure 1. Schematic diagram of surface analysis system used for silver/oxygen surface characterization studies.

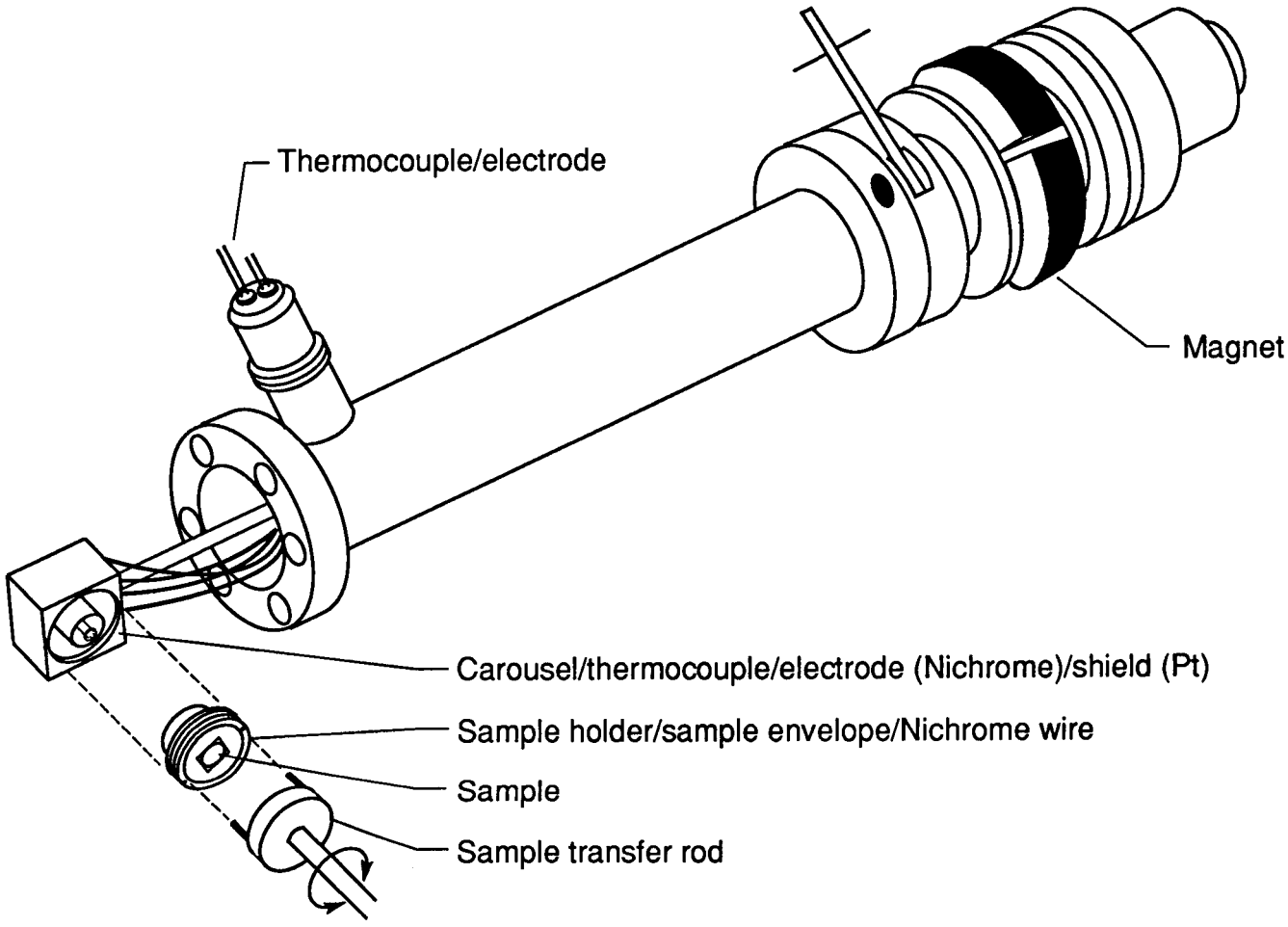

Figure 2. Schematic diagram of detail of heater assembly in the sample introduction/preparation chamber.

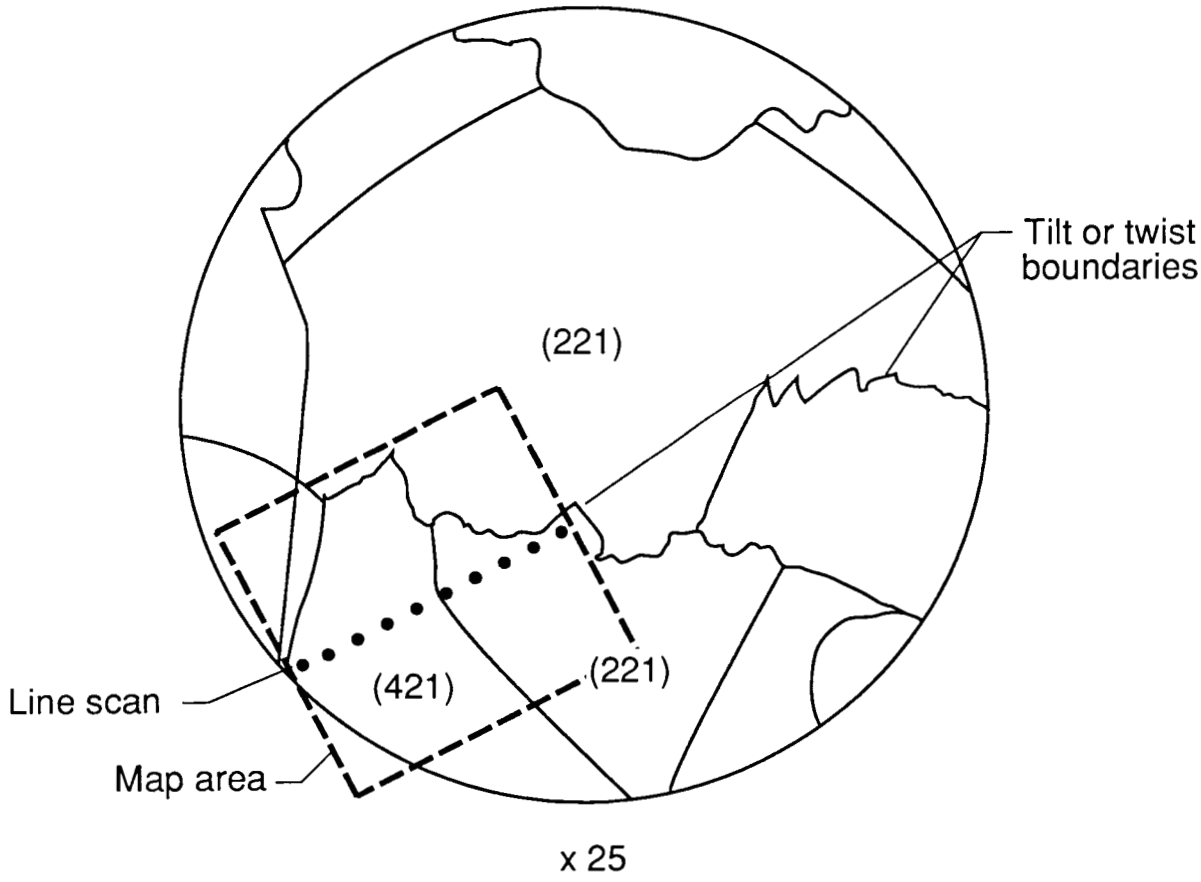

Figure 3. Tracing of the grain boundaries of the polycrystalline silver sample. Dashed region encloses area studied and dotted line is location of line scans.

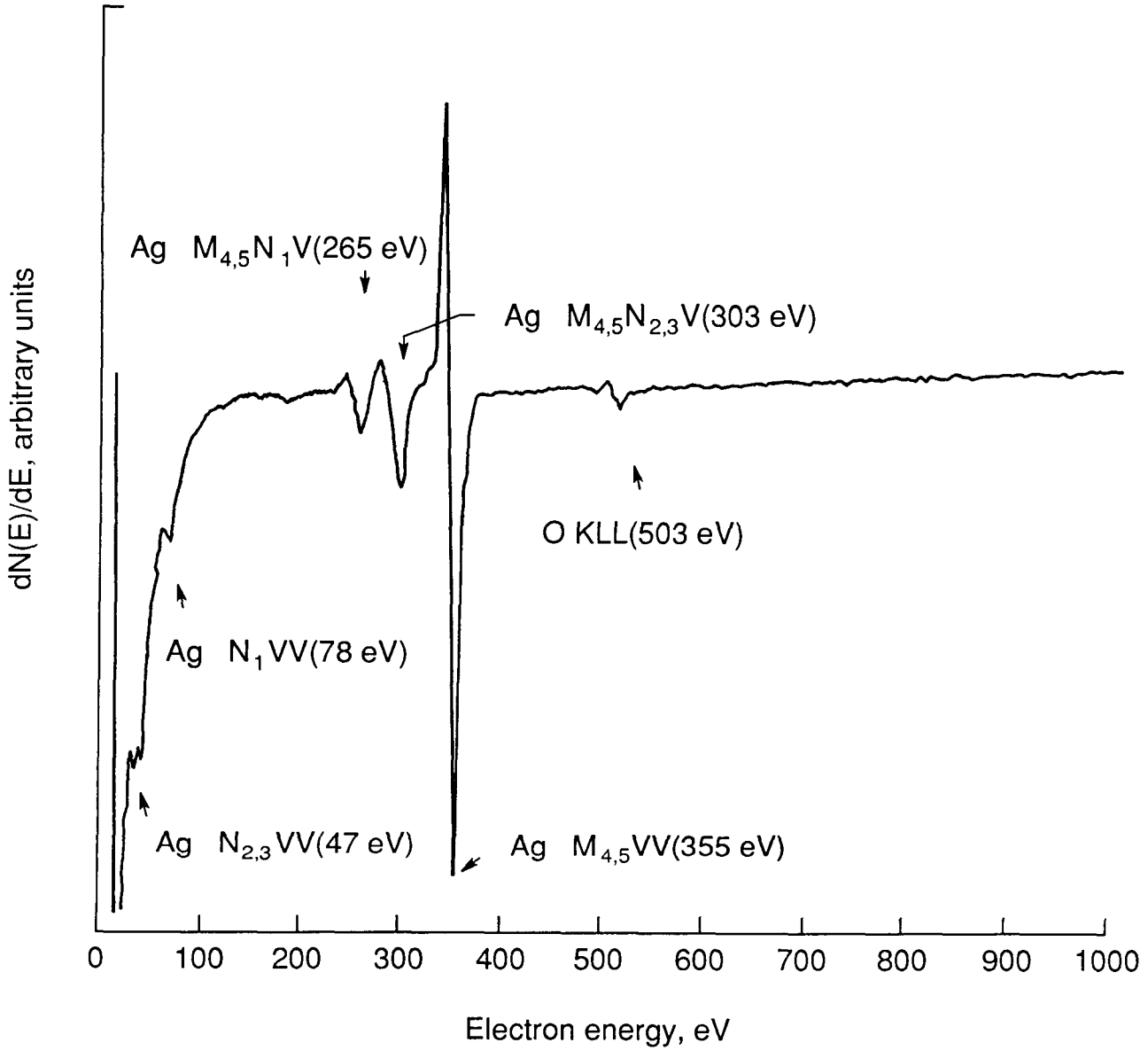

Figure 4. Auger spectrum of the silver sample cleaned by argon ion bombardment after charging oxygen in 100-torr oxygen at 600°C for 2 hr; normal incidence; primary electron beam energy $E_P = 2000$ eV; primary beam current $I_p = 1.3$ μA; modulation voltage 5 V.

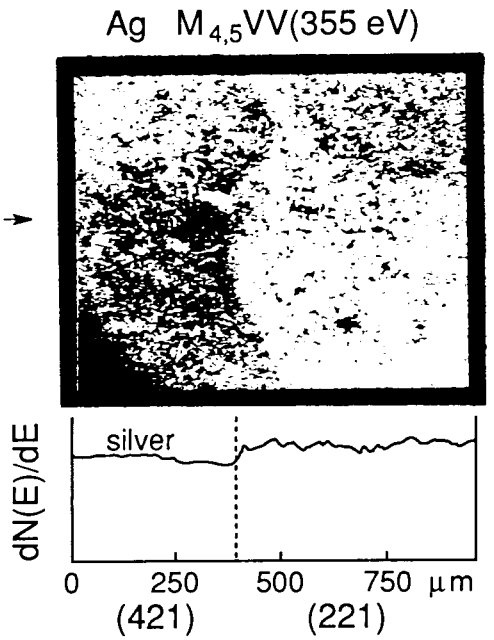

(a) Ag $M_{4,5}VV$ after cleaning by ion bombardment.

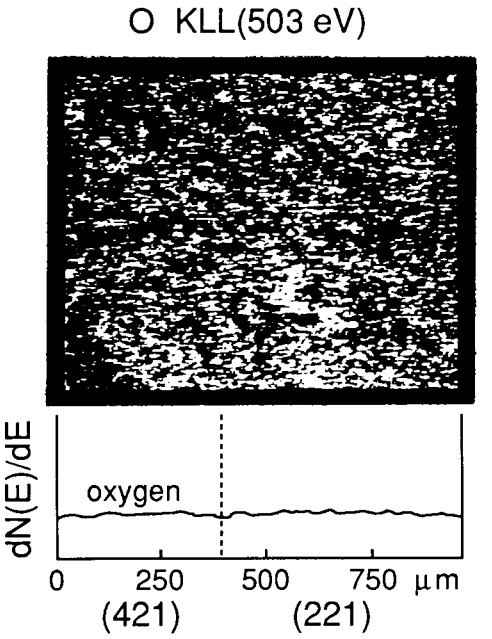

(b) O KLL after cleaning by ion bombardment.

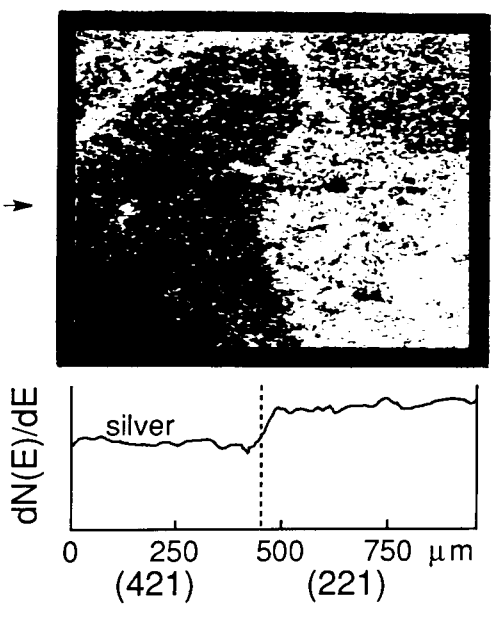

(c) Ag $M_{4,5}VV$ after heating at 470° in UHV for 30 min.

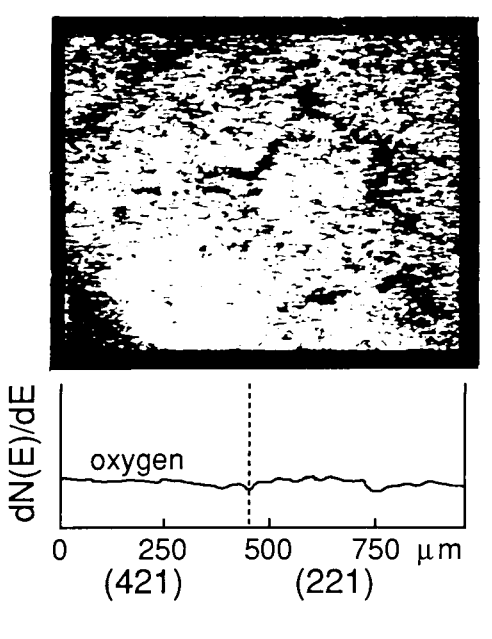

(d) O KLL after heating at 470°C in UHV for 30 min.

Figure 5. Auger images and line scans of silver $M_{4,5}VV$ (355 eV) and O KLL (503 eV). Arrows indicate the position of line scans. Dashed lines represent position of grain boundary. Normal incidence; $E_p = 3000$ eV; $I_p = 0.1$ μA; modulation 10 V.

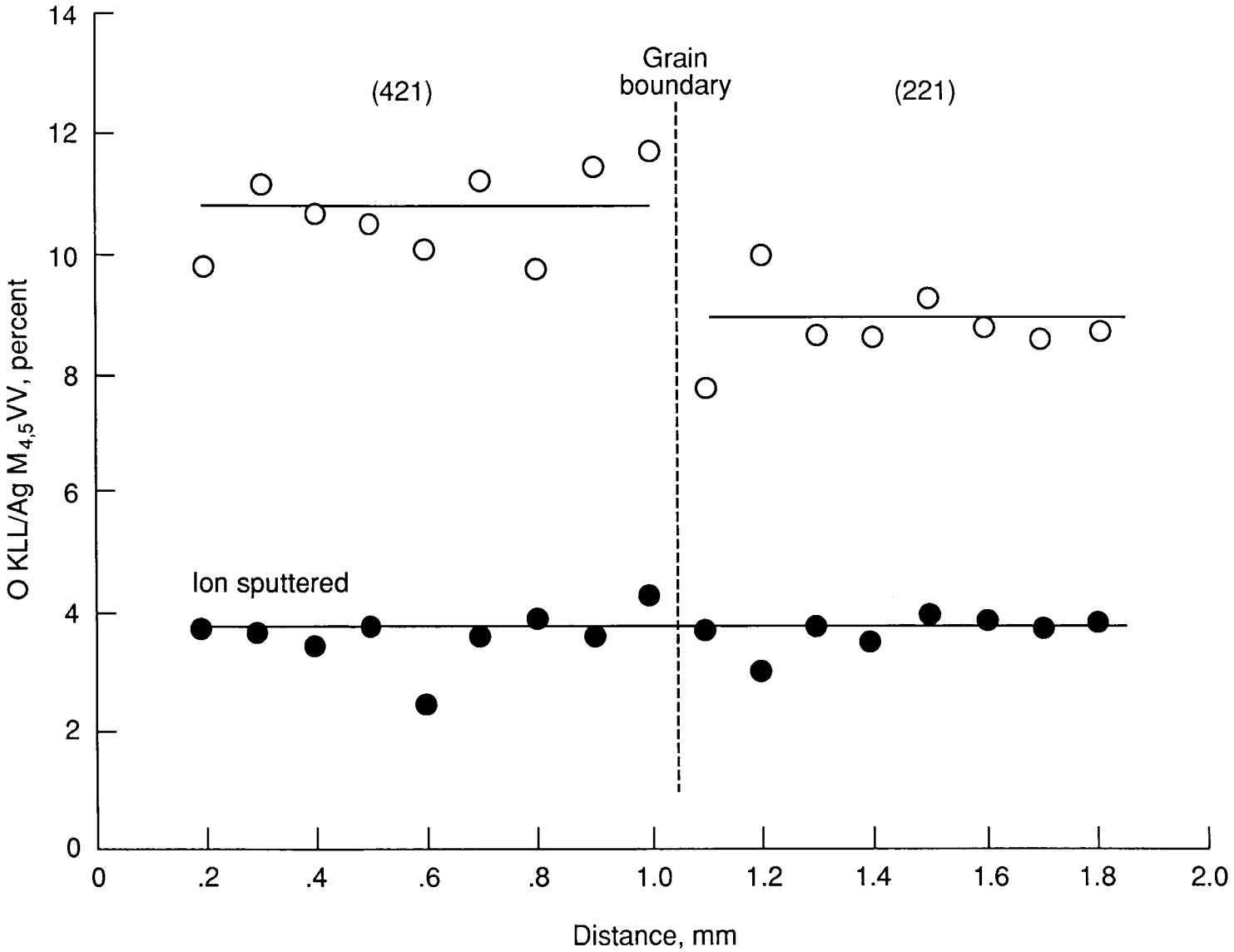

Figure 6. Variation of oxygen-to-silver ($M_{4,5}VV$) peak ratio with different grains. Solid circles indicate oxygen-to-silver ratio after cleaning by ion bombardment; open circles indicate oxygen-to-silver ratio after heating at 470°C in UHV for 30 min.

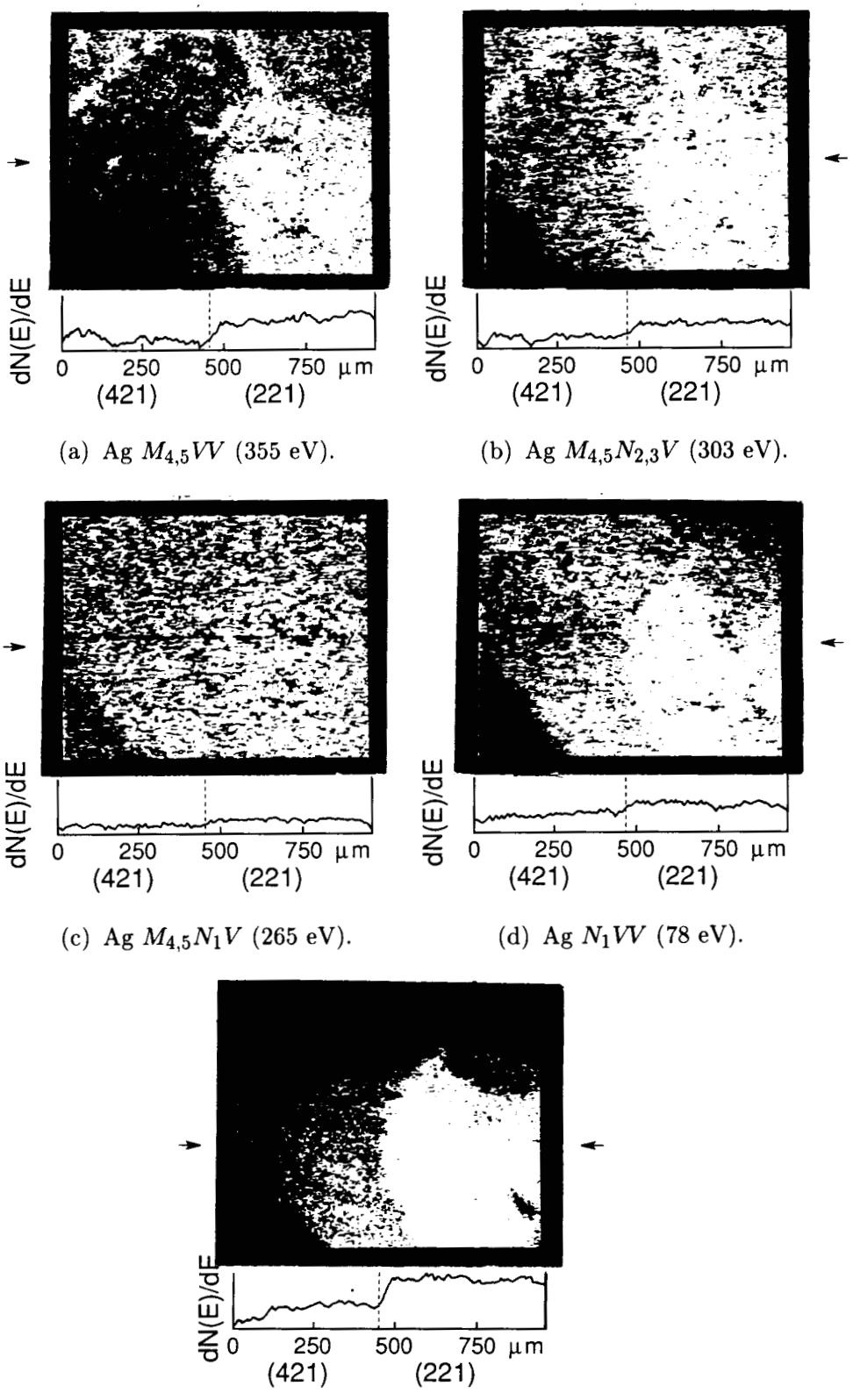

(a) Ag $M_{4,5}VV$ (355 eV).

(b) Ag $M_{4,5}N_{2,3}V$ (303 eV).

(c) Ag $M_{4,5}N_1V$ (265 eV).

(d) Ag N_1VV (78 eV).

(e) Ag $N_1N_{2,3}V$ (27 eV).

Figure 7. Auger images and line scans of the different silver Auger transitions. Arrows indicate the position of line scans. Dashed lines represent position of grain boundary. Normal incidence; E_p = 3000 eV; I_p = 1.0 μA; modulation 10 V.

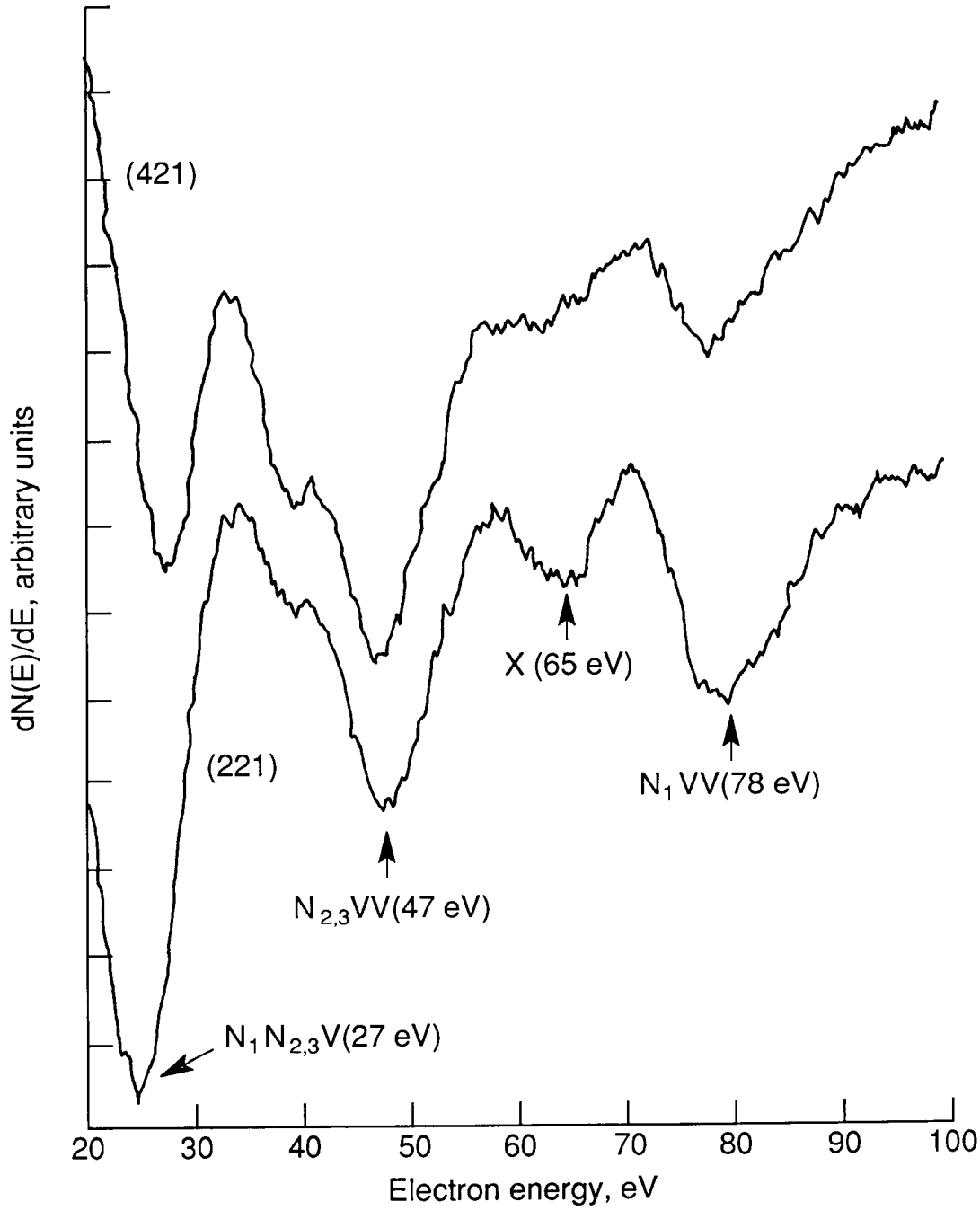

Figure 8. Auger spectra (20–100 eV) of the (421) and the (221) grains of figure 3. Normal incidence; E_p = 3000 eV; I_p = 1.0 μA; modulation 10 V.

NASA
National Aeronautics and Space Administration

Report Documentation Page

1. Report No.	2. Government Accession No.	3. Recipient's Catalog No.
NASA TP-2930		

4. Title and Subtitle	5. Report Date
Auger Electron Intensity Variations in Oxygen-Charged Large Grain Polycrystalline Silver	October 1989
	6. Performing Organization Code
7. Author(s)	8. Performing Organization Report No.
W. S. Lee, R. A. Outlaw, G. B. Hoflund, and M. R. Davidson	L-16579
9. Performing Organization Name and Address	10. Work Unit No.
NASA Langley Research Center Hampton, VA 23665-5225	307-51-08-04
	11. Contract or Grant No.
12. Sponsoring Agency Name and Address	13. Type of Report and Period Covered
National Aeronautics and Space Administration Washington, DC 20546-0001	Technical Paper
	14. Sponsoring Agency Code

15. Supplementary Notes

W. S. Lee: Hampton University, Hampton, Virginia.
R. A. Outlaw: Langley Research Center, Hampton, Virginia.
G. B. Hoflund and M. R. Davidson: University of Florida, Gainesville, Florida.

16. Abstract

Auger electron spectroscopic studies of the grains in oxygen-charged polycrystalline silver show significant intensity variations as a function of crystallographic orientation. These intensity variations have been observed in studies of the Auger images and line scans of the different grains (randomly selected) for each silver transition energy. The results can be attributed to the diffraction of the ejected Auger electrons and interpreted by corresponding changes in the electron mean free path for inelastic scattering and by oxygen atom accumulation in the subsurface. The subsurface (second layer) octahedral sites have increased in size because of surface relaxation and serve as a stable reservoir for the dissolved oxygen.

17. Key Words (Suggested by Authors(s))	18. Distribution Statement
Auger electron spectroscopy Auger images Electron diffraction Inelastic mean free path	Unclassified—Unlimited Subject Category 72

19. Security Classif. (of this report)	20. Security Classif. (of this page)	21. No. of Pages	22. Price
Unclassified	Unclassified	16	A03

NASA-Langley, 1989

For sale by the National Technical Information Service, Springfield, Virginia 22161-2171